IOP Publishing Phys. Med. Biol. 71 (2026) 085015 https://doi.org/10.1088/1361-6560/ae6018

Physics in Medicine & Biology

IPEM Institute of Physics and Engineering in Medicine

OPEN ACCESS

RECEIVED
12 December 2025

REVISED
23 March 2026

ACCEPTED FOR PUBLICATION
14 April 2026

PUBLISHED
24 April 2026

PAPER

Monte Carlo and film dosimetry study of collimator effects on penumbra and out-of-field dose for very high-energy electrons

Jade Fischer[1,*], Antonio Gilardi[2], Alexander Malyzhenkov[2], Pierre Korysko[3], Alexander Hart[1], Vilde Rieker[4], Joseph Bateman[3], Wilfrid Farabolini[2], Roberto Corsini[2], Manjit Dosanjh[3] and Magdalena Bazalova-Carter[1]

[1] Department of Physics and Astronomy, University of Victoria, Victoria, Canada
[2] CERN, Geneva, Switzerland
[3] Department of Physics, University of Oxford, Oxford, United Kingdom
[4] Department of Physics, University of Oslo, Oslo, Norway
[*] Author to whom any correspondence should be addressed.

E-mail: jadefischer@uvic.ca

Keywords: Monte Carlo simulations, film dosimetry, radiotherapy, very-high energy electrons, collimation

Abstract

Objective. Very high-energy electrons (VHEEs) offer deep penetration, low scattering, and the potential for ultra-high dose rate delivery, making them promising candidates for future radiotherapy. However, the collimation of VHEE beams to achieve sharp beam penumbra remains poorly characterized. This study experimentally and computationally investigates how collimator material, thickness, and beam characteristics affect penumbra and out-of-field dose for VHEEs and establishes an initial foundation for the design of clinically feasible VHEE collimators. *Approach.* Tungsten, lead, and brass 5 mm diameter collimators were evaluated using film dosimetry with a 200 MeV electron beam delivered at the CERN Linear Electron Accelerator for Research and validated through Monte Carlo (MC) simulations. Experimental measurements of penumbra and out-of-field dose were compared with simulations that systematically varied material (tungsten, lead, brass), thickness (20–80 mm), and beam energy (150–250 MeV). Additional sensitivity tests quantified the impact of beam instability on field shaping. *Main results.* For measurements in air, penumbrae increased linearly with distance from the collimator and was smallest for tungsten. Out-of-field dose decreased with increasing thickness, falling below 0.5% for a 40 mm thick tungsten collimator. Brass exhibited the highest out-of-field dose (up to 4.8%) and broadest penumbra. MC models reproduced experimental trends within 5% for penumbrae but underestimated out-of-field dose, particularly for brass. The simulations indicated that VHEE beam divergence, beam size and collimator misalignment strongly influence beam penumbra and out-of-field dose. *Significance.* The presented work demonstrates that collimator material and geometry play a critical role in defining VHEE beam quality. Tungsten provided optimal attenuation and sharpness compared to brass and lead. These results establish quantitative benchmarks for VHEE collimator design and emphasize the importance of beam stability.

1. Introduction

Very high-energy electrons (VHEEs) are becoming a promising option for radiotherapy due to their unique physical and dosimetric properties (Fischer *et al* 2024). By raising the energy of clinical electron beams (4–20 MeV) to the range of VHEEs (>100 MeV), it becomes possible to target deep-seated tumors in the thorax, abdomen, or pelvis (DesRosiers *et al* 2000, Bazalova-Carter *et al* 2015, Palma *et al* 2016, Schuler *et al* 2017). VHEEs also produce less lateral scatter and show low sensitivity to variations in tissue density (Papiez *et al* 2002, Glinec *et al* 2006). One major reason for the continued interest in VHEEs is their ability to be delivered at ultra-high dose rates (UHDR). UHDR delivery has demonstrated the ability to spare normal tissue while preserving tumor control (Zhou 2020). Early experimental work has

shown that VHEEs can deliver dose rates on the order of 10^9 Gy s^{-1} (Clements *et al* 2023, Hart 2024). In recent years, the field is moving towards the clinical implementation of VHEEs, and THERYQ is currently developing a compact VHEE-based treatment system called FLASHDEEP (Fischer *et al* 2024). According to the available description, the proposed design is expected to be more compact than conventional proton therapy systems, which typically require cyclotrons or synchrotrons and large gantries for multi-beam delivery. (Robertson *et al* 2026). With the reduction in size and potential for reduction in shielding, a VHEE machine may provide a UHDR option which could be more cost-effective compared to UHDR proton therapy (Li *et al* 2024).

As efforts progress toward clinical implementation, one of the most critical questions for VHEEs is how to best shape and deliver the beam to achieve high-quality dose distributions. The development of effective and clinically practical collimators should be an essential step in establishing VHEEs as a viable modality. For electrons in the current clinical energy range, customized cutouts are typical, although low-energy scatter is a key concern, and cutouts must be placed within <5 cm of the patient's body (Jursinic 1997, Maharaj *et al* 2024, Lee *et al* 2025).

For VHEEs, collimation may play an equally critical role, particularly given the various approaches currently proposed for beam delivery: pencil beam scanning (PBS), double-scattered systems (Ronga *et al* 2021) and magnetic focusing. PBS employs fast magnets to deliver the dose spot by spot, which results in highly conformal dose distributions. In proton therapy, collimators have been proposed in conjunction with PBS to sharpen edges and improve conformity (Hyer *et al* 2021). The primary drawback of PBS is that the technique presents complexity in design and installation. In contrast, collimated double-scattered systems deliver an entire field at once (Zhang *et al* 2021). Double-scattering simplifies the delivery process by avoiding the need for rapid steering magnets (Farr *et al* 2022). These features make collimated VHEE delivery straightforward, reliable, and reproducible which is essential for new therapies in translational development (Ronga *et al* 2021). Magnetic focusing uses a set of quadrupoles to focus the electron beam at a specific location within the patient. Focused VHEE beams can produce improved lateral penumbra and reduce the high entrance dose that is characteristic of VHEEs (Whitmore *et al* 2021, 2024). However, such approaches require complex beam optics and accelerator infrastructure. In contrast, mechanical collimation provides a simpler method for shaping VHEE beams, particularly in early-stage experimental systems.

While collimation may be an important aspect of VHEE implementation, it is poorly understood. For VHEEs, multiple Coulomb scattering at the collimator edges will broaden the penumbra, an effect that has yet to be examined. Material choice is another factor in collimator design, as high atomic number (Z) materials can generate substantial bremsstrahlung contamination that contributes to out-of-field dose. In contrast, low atomic number materials may require impractically large thicknesses to adequately attenuate the primary beam. Systematic simulations or experimental characterization of VHEE collimation has not yet been reported, leaving a gap in our understanding of how to design collimators for a VHEE system.

The aim of this work was to perform the first experimental investigation of VHEE collimation using collimators of varying materials. This study characterized out-of-field dose, and penumbra sharpness using radiochromic films at the CERN Linear Electron Accelerator for Research (CLEAR). Complementary Monte Carlo (MC) simulations were used to model bremsstrahlung production and generalize the findings beyond experimental conditions. Furthermore, these simulations investigated the impact of beam characteristics on penumbra and out-of-field dose. Together, these results provide systematic insight into collimator performance for VHEE radiotherapy and establish a foundation for translating this modality toward clinical application.

2. Materials and methods

2.1. Experimental set-up at CLEAR

All measurements were carried out at CLEAR, a user facility dedicated to accelerator physics, medical physics, and industrial applications. CLEAR is capable of accelerating electron beams up to 220 MeV, making it one of the few facilities worldwide able to produce very high-energy electrons (VHEEs) under controlled experimental conditions (Fischer *et al* 2024). The accelerator delivers beams with a highly flexible time structure: picosecond-length electron bunches which are produced at gigahertz frequencies and can be grouped into trains operating from sub-hertz repetition rates up to 10 Hz (Korysko *et al* 2023).

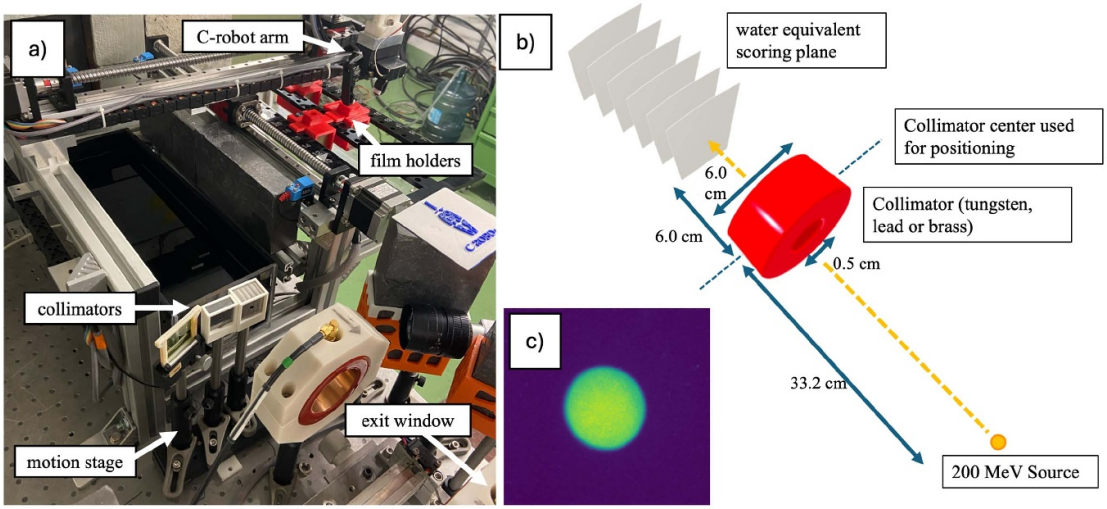

Figure 1. (a) Photograph of the experimental setup installed at CLEAR which was used to irradiate radiochromic film. Multiple materials (tungsten, brass and lead) with thicknesses of 20–40 mm were tested. (b) Simulation configuration for modeling the CLEAR irradiations. (c) Example of the experimental dose distribution produced by passing the Gaussian beam through a collimator.

This flexibility allows experiments to replicate both conventional and UHDR conditions, providing a unique platform for preclinical and dosimetric investigations.

Three collimators were evaluated: a 20 mm thick tungsten collimator, a 20 mm thick lead collimator, and a 40 mm thick brass collimator. Tungsten, lead, and brass were selected as collimator materials due to their common use in radiotherapy collimation (Boyer *et al* 2001, Chen *et al* 2014, Law *et al* 2025). These materials span a representative range of densities and atomic numbers relevant for beam collimation. The brass collimator was manufactured with a thickness of 40 mm to compensate for its lower atomic number and density relative to tungsten and lead, which result in reduced VHEE beam attenuation. Each was constructed with a 30 mm × 30 mm face and a 5 mm diameter parallel bore through the center. The collimators were mounted in custom 3D-printed holders secured to a motorized motion stage, allowing them to be moved into position for each irradiation. The collimator center was positioned 332 mm downstream from the CLEAR beamline exit window and aligned to the beam axis using a laser. The setup for the experimental measurements is shown in figure 1.

The 35 × 40 mm films were mounted in custom-made 3D-printed holders and suspended in air. The film holder positioned the first film 60 mm downstream from the center of the collimator. Four or six films were used per irradiation, positioned between 60 and 110 mm from the collimator to evaluate dose distribution as a function of distance from the collimator. At each irradiation, an additional film was placed outside the beam path to record background radiation. The measured background dose was subtracted from all the irradiated films.

All irradiations were conducted using a 200 MeV beam, targeting a dose of 10 Gy. To this end, charges of 6.0 nC was delivered for the tungsten and lead collimators, and 6.2 nC for the brass collimator. All irradiations were performed using a repetition rate of 0.833 Hz.

The experimental nature of the CLEAR beamline presents uncertainty in dose delivered per charge, beam size and beam positioning. Previous studies have shown significant day-to-day variations, as well as variations occurring throughout a given day (Giguére *et al* 2025). To account for these variations, an open uncollimated beam measurement was acquired each day. These measurements included six films spaced at 10 mm with positioning identical to collimator experiments. The open beam measurements were intended to capture variations in beam alignment, beam size, or beam divergence between experimental sets acquired on different days. However, they could not account for fluctuations occurring within a single day. These fluctuations may lead to small differences in the measured dose distribution compared with that predicted from the corresponding open beam measurement.

2.2. Film dosimetry

Film dosimetry was performed using Gafchromic EBT3 radiochromic films (Ashland Inc. Wayne, NJ, USA). The films were calibrated to dose-to-water using a 5.5 MeV electron beam (Oriatron eRT6) at a dose rate of 0.05 Gy s^{-1}. Following irradiation, the films were stored for 24 h to allow for post-exposure polymerization and then digitized using an Epson Perfection V800 flatbed scanner (Suwa, Japan) at a

resolution of 300 dpi. Net optical density (*netOD*) was calculated from the red channel by taking the logarithm of the ratio of pixel intensities between background and exposed films. The resulting *netOD* values were converted to dose through a calibration curve described by equation (1):

$$netOD = (a + b * D) / (D + c), \quad (1)$$

where a, b, and c are constants determined through calibration of the film and D is the delivered absorbed dose. EBT3 has been widely used in VHEE research due to its combination of high spatial resolution, near water-equivalence, and robustness against changes in dose rate. Previous investigations have demonstrated that EBT3 response remains stable up to UHDRs of 8×10^6 Gy s^{-1} (Jaccard *et al* 2017) and was energy independent for electrons up to 165 MeV (Subiel 2014). Multiple studies have validated its performance under FLASH conditions and report agreement with reference detectors within a few percent (Sorriaux *et al* 2013, Bazalova-Carter 2015, Clements 2024). An additional uncertainty of 2.5% was included in the experimental dose measurements to account for the reported response difference of radiochromic film when calibrated at low electron energies (5 MeV) and irradiated with 200 MeV VHEEs (Clements 2024).

2.3. Analysis of dose distributions

To evaluate collimated dose distributions from experimental measurements and MC simulations (detailed in section 2.4), custom Python tools were developed to calculate penumbra and out-of-field dose. The center of mass of the circular dose distribution was first identified, and radial profiles were extracted at 12° intervals. For each profile, the 20%–80% beam penumbra was calculated. Additionally, out-of-field dose was calculated for all dose distributions. Out-of-field dose refers to dose outside the intended field arising from transmission through the collimator and from secondary radiation produced within it. Out-of-field dose was quantified by averaging the dose within an annular region surrounding the peak dose area. This region had an inner edge located 5 mm from the center of the dose distribution and a thickness of 3.5 mm. The out-of-field dose was normalized to the the peak dose delivered to the film located at 60 mm from the collimator. The transverse dose distributions of uncollimated open beams were evaluated by fitting dose profiles to a Gaussian function, yielding the peak dose and beam size defined by σ of the Gaussian beam.

2.4. MC simulations

2.4.1. Simulation setup

MC simulations were performed using TOPAS version 3.9 (Perl *et al* 2012, Faddegon *et al* 2020). Collimator size and material were varied, but the collimator position remained fixed, defined relative to its center. The simulation geometry was designed to replicate the experimental setup. The VHEE source was positioned 332 mm upstream from the center of the collimator, and the first film was placed 60 mm downstream from the collimator . Films were modeled as 0.3 mm thick water slabs and 6 films were placed at 10 mm intervals. Dose was scored with the same resolution as the scanned EBT3 films, resulting in voxel dimensions of 0.085 mm × 0.085 mm.

The collimator was modeled as a 60 mm diameter cylinder with a 5 mm bore in the center. This configuration produced results equivalent to a square collimator matching the experimental setup while reducing the geometric complexity of the model by eliminating the need for overlapping geometries.

A set of well-established physics libraries for VHEEs was utilized for this work: g4em-standard-opt4, g4em-extra, g4h-elastic_HP, g4ion-binarycascade, g4h-phy_QGSP_BIC_HP, g4decay, g4radioactivedecay and g4stopping (Clements *et al* 2024, Fischer *et al* 2024, Ronga *et al* 2025). The range cut was set to 0.005 mm to accurately model secondary particle production and transport in the steep dose gradients created by the narrow 5 mm bore holes of the collimator. To further improve spatial resolution in these high-gradient regions, the maximum step size within the collimator aperture was restricted to 0.01 mm. Simulations took from 6 to 10 h and were completed on a Compute Canada cluster with 64 CPUs (2.40 GHz).

2.4.2. Parameter study

Due to significant variations in the experimental open beam measurements at CLEAR, which showed distinctly different beam characteristics between irradiations, the experimental data alone were insufficient to evaluate the effects of collimator material or thickness on the resulting dose distributions. For this reason, a set of comprehensive MC simulations were conducted to investigate the impact of material, thickness, and beam energy on beam penumbra and out-of-field dose.

The incident beam was representative of the CLEAR beamline and modeled as a symmetric Gaussian source with a beam size of $\sigma = 3.83$ mm and an angular divergence of 0.21° with 1×10^7 primary electrons. The resulting beam has $\sigma = 4.05$ mm at the collimator.

A set of simulations were run with varying collimator material (tungsten, lead, brass), thickness (20–40 mm) and incident beam energy (150–250 MeV). The effects of collimator thicknesses were investigated with all collimator materials for a 200 MeV beam, while energies of 150, 200 and 250 MeV were investigated with the same materials for a 40 mm thick collimator. Although the CLEAR beamline operates up to 220 MeV, energies up to 250 MeV were considered in this study to remain consistent with the broader VHEE literature, which frequently investigates this energy range (DesRosiers *et al* 2000, Papiez *et al* 2002, Yeboah *et al* 2002).

To expand upon the measurement of penumbra in air, these simulations were repeated with the inclusion of a $300 \times 300 \times 300$ mm^3 water phantom located at 38 mm downstream from the collimator. The first film was positioned at a depth of 22 mm, with subsequent films positioned in 10 mm increments up to a depth of 72 mm. For these simulations, all other beam parameters match the in air parameter setup and the explored parameter space was the same.

2.4.3. Experimental beam modeling

Open beam measurements were used to develop the individualized MC beam model for each collimator. Small adjustments were made to the beam size (σ) and angular divergence until agreement was achieved between the penumbra of the simulated and measured dose profiles from film. This procedure was repeated for each collimator irradiation to produce a corresponding MC beam model.

Using the MC model developed for each collimator, simulations were run where a phase-space file was scored 5 mm from upstream and downstream from the face of the collimator. The beam along the central axis (CAX) was investigated in a region of interest of 5×5 mm^2 aligned with CAX. Only forward-propagating particles were included in the analysis. The resulting spectra were used to characterize the energy distributions of photons and electrons. The energy distribution was converted to a probability density function, which was then scaled by the fractional contribution of each particle type to the total forward-going particle population.

In the next step, the contribution of bremsstrahlung photon and neutron dose attributed to the collimator was evaluated. Separate simulations were performed for bremsstrahlung photons and secondary neutrons to isolate their individual dose contributions. Dose was scored in six film planes placed at 10 mm intervals downstream of the collimator, consistent with the reference simulation setup, and evaluated according to the procedure described in section 2.3. The resulting bremsstrahlung photon and neutron doses in the out-of-field region were evaluated relative to the total out-of-field dose and relative to the CAX dose to express their contributions as a percentage of the peak beam dose.

2.4.4. Beam sensitivity tests

A brief beam sensitivity study was conducted, demonstrating the impact of various beam parameters on penumbra with the same collimator. A parameter study is presented for the 20 mm thick tungsten collimator to demonstrate the effect of collimator misalignment (perpendicular and parallel to beam axis), beam size (σ) and beam divergence.

To isolate beam divergence, a variety of beam models were developed in which a beam size of $\sigma = 4.0$ mm at the collimator was achieved. The angular divergence range investigated extended from 0.01° to 0.4°.

For the beam size tests, the beam size refers to the standard deviation (σ) of the Gaussian distribution describing the transverse particle positions at the source plane. The beams were modeled as parallel with zero divergence, and the beam sizes investigated had σ values ranging from 3.0 mm to 6.0 mm. Additionally, perpendicular collimator offsets from 0 to 3 mm were investigated. For the parallel misalignment simulations, the collimator was shifted up to 15 mm towards (+) or away (−) from the film. In these misalignment simulations, the beam was modeled with no divergence and a beam size of $\sigma = 4.0$ mm. With zero beam divergence, the beam size (defined by σ of the Gaussian beam) remains the same at both the source and the collimator for the divergence, perpendicular offset, and parallel offset tests. A full set of parameter values is shown in table 1.

Table 1. Summary of beam parameter variations used in the beam sensitivity study.

	Parameter settings			
	Divergence (degree)	Sigma (mm)	Perpendicular offset (mm)	Parallel offset (mm)
Divergence	0.1–0.4	4.0 (at collimator)	0	0
Sigma	0	3.0–6.0	0	0
Perpendicular offset	0	4.0 (at source)	0.0–3.0	0
Parallel offset	0	4.0 (at source)	0	−1.5–1.5

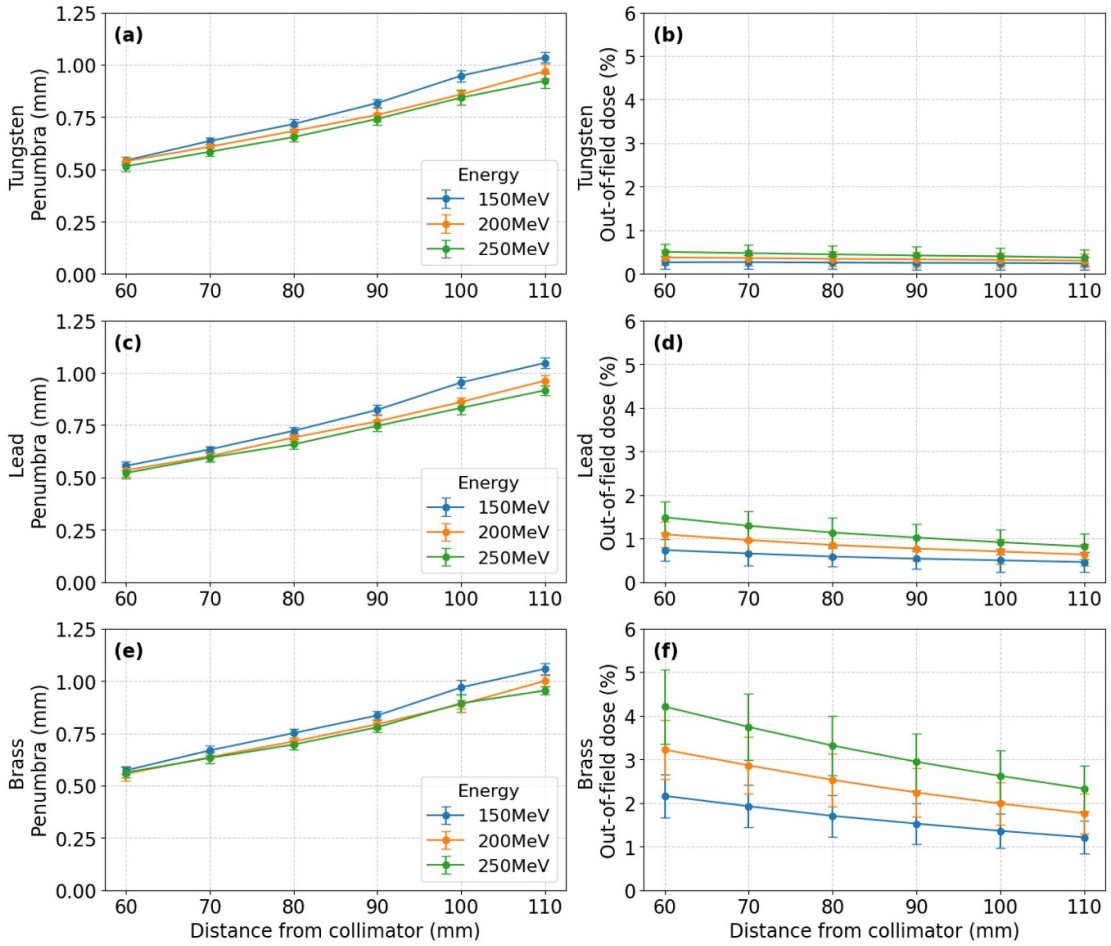

Figure 2. Panels (a), (c), (e) on the left show the penumbra widths, while panels (b), (d), (f) on the right display the out-of-field dose as a function of distance from the collimator for tungsten (a), (b), lead (c), (d), and brass (e), (f) collimators at 150, 200, and 250 MeV in air, calculated using MC simulations.

3. Results

3.1. Parameter study

MC simulation results of VHEE beam penumbrae and out-of-field dose, evaluated in air for tungsten, lead, and brass collimators at 150, 200, and 250 MeV, are shown in figure 2. As expected, penumbrae increased with distance from the collimator for all materials and energies. Among all collimator materials, the penumbrae increased the most for the lowest energy (150 MeV) beam.

At a distance of 60 mm from the collimator, the penumbrae ranged from to 0.51 ± 0.02 mm (tungsten, 250 MeV) to 0.57 ± 0.02 mm (brass, 150 MeV), increasing to a maximum of 1.05 ± 0.03 mm at 110 mm for brass at 150 MeV. Tungsten consistently produced the sharpest penumbra with values remaining below 0.54 mm across all energies at 60 mm from the collimator.

The out-of-field dose was lowest for tungsten, remaining below $0.5 \pm 0.2\%$ of the peak dose across all conditions, and exhibited minimal variation over the investigated distance. In the 250 MeV case, the out-of-field dose at 60 mm was $0.5 \pm 0.2\%$ and only decreased to $0.4 \pm 0.2\%$ by the 110 mm position. Lead out-of-field dose ranged from $0.7 \pm 0.2\%$ for 150 MeV to $1.4 \pm 0.3\%$ for 250 MeV at 60 mm

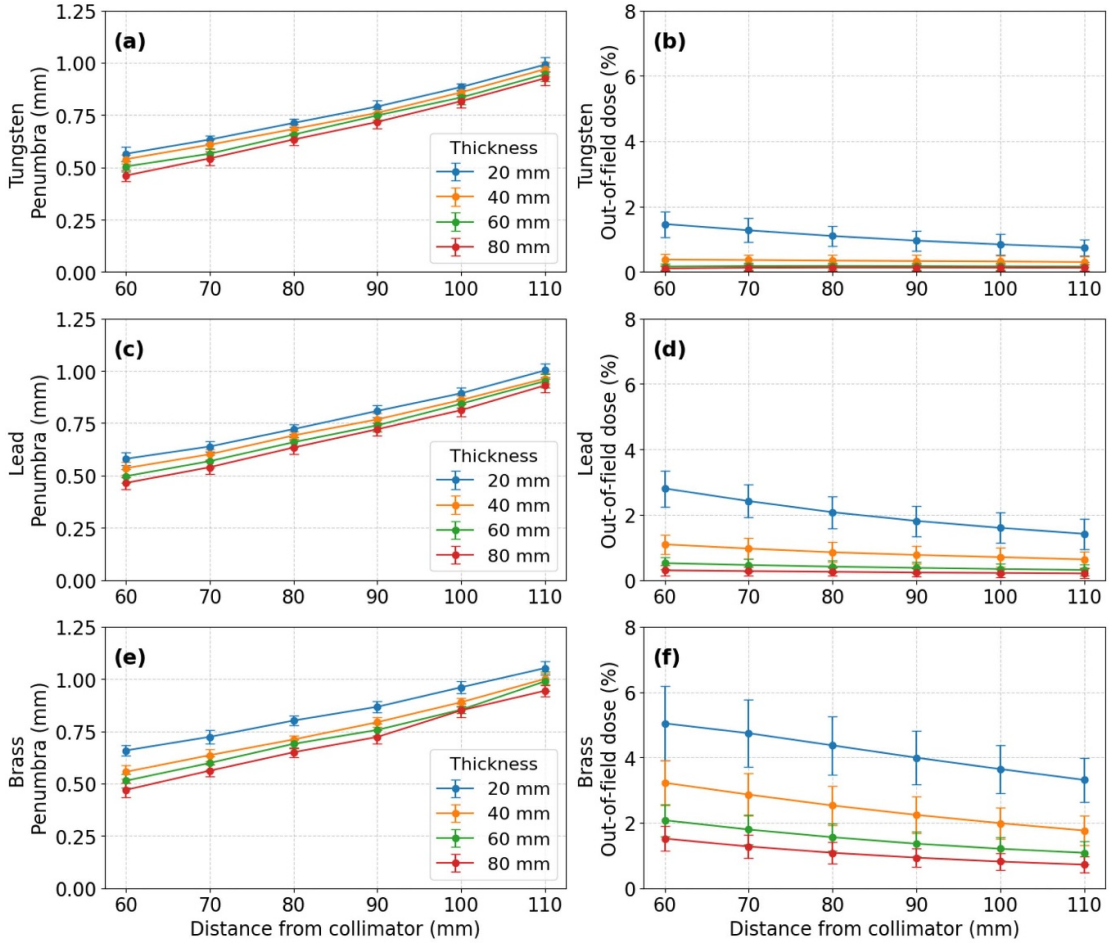

Figure 3. Panels (a), (c), (e) on the left show the penumbra widths, while panels (b), (d), (f) on the right display the out-of-field dose as a function of distance from the collimator for tungsten (a), (b), lead (c), (d), and brass (e), (f) collimators with different thicknesses in air, based on MC simulations.

from the collimator. Brass showed the greatest out-of-field dose, reaching $4.2 \pm 0.8\%$ at 60 mm for the 250 MeV case and decreasing to $2.3 \pm 0.5\%$ at 110 mm. At 150 MeV, the out-of-field dose was $2.2 \pm 0.5\%$ at 60 mm from the collimator and dropped to $1.2 \pm 0.4\%$ at 110 mm.

Beam penumbra and out-of-field dose were evaluated in air across four collimator thicknesses (20, 40, 60, and 80 mm) for tungsten, lead, and brass (figure 3). Penumbra exhibited a weaker dependence on collimator thickness compared to out-of-field dose. All reductions in the penumbrae were under 0.18 mm between the thinnest and thickest configurations. At 60 mm from the collimator, the penumbra for tungsten ranged from 0.56 ± 0.03 mm (20 mm collimator) to 0.46 ± 0.03 mm (80 mm collimator). Lead mirrored the results of tungsten with penumbrae ranging from 0.57 ± 0.03 mm (20 mm collimator) to 0.46 ± 0.02 mm (80 mm collimator). Brass demonstrated poorer collimation for lower thicknesses with a penumbra of 0.65 ± 0.02 mm for a 20 mm thick collimator. Once the thickness of the brass collimator was increased to 80 mm, the penumbra was found to be comparable to lead and tungsten at 0.46 ± 0.02 mm. Increasing thickness consistently reduced out-of-field dose for all materials. For tungsten, the out-of-field dose decreased from $1.5 \pm 0.4\%$ at 20 mm thickness to $0.10 \pm 0.07\%$ at 80 mm thickness. Lead followed a similar trend, with the out-of-field dose decreasing from $2.8 \pm 0.5\%$ to $0.3 \pm 0.2\%$, while brass exhibited the highest out-of-field dose, decreasing from $5.0 \pm 1.1\%$ at 20 mm to $1.5 \pm 0.4\%$ at 80 mm.

When measured in water (figure 4), all collimator materials exhibited a broader penumbra and slightly higher out-of-field dose compared to simulations in air. For the tungsten collimator, the penumbra increased from 0.82 ± 0.03 mm at 22 mm to 2.26 ± 0.06 mm at a depth of 110 mm in water. Out-of-field dose for the tungsten collimator decreased with distance from the collimator from $1.8 \pm 0.4\%$ to $1.1 \pm 0.3\%$ of the peak dose. For the lead collimator, the penumbrae ranged from 0.85 ± 0.02 mm at 22 mm depth to 2.36 ± 0.05 mm at 132 mm depth in water. While lead out-of-field dose decreased from

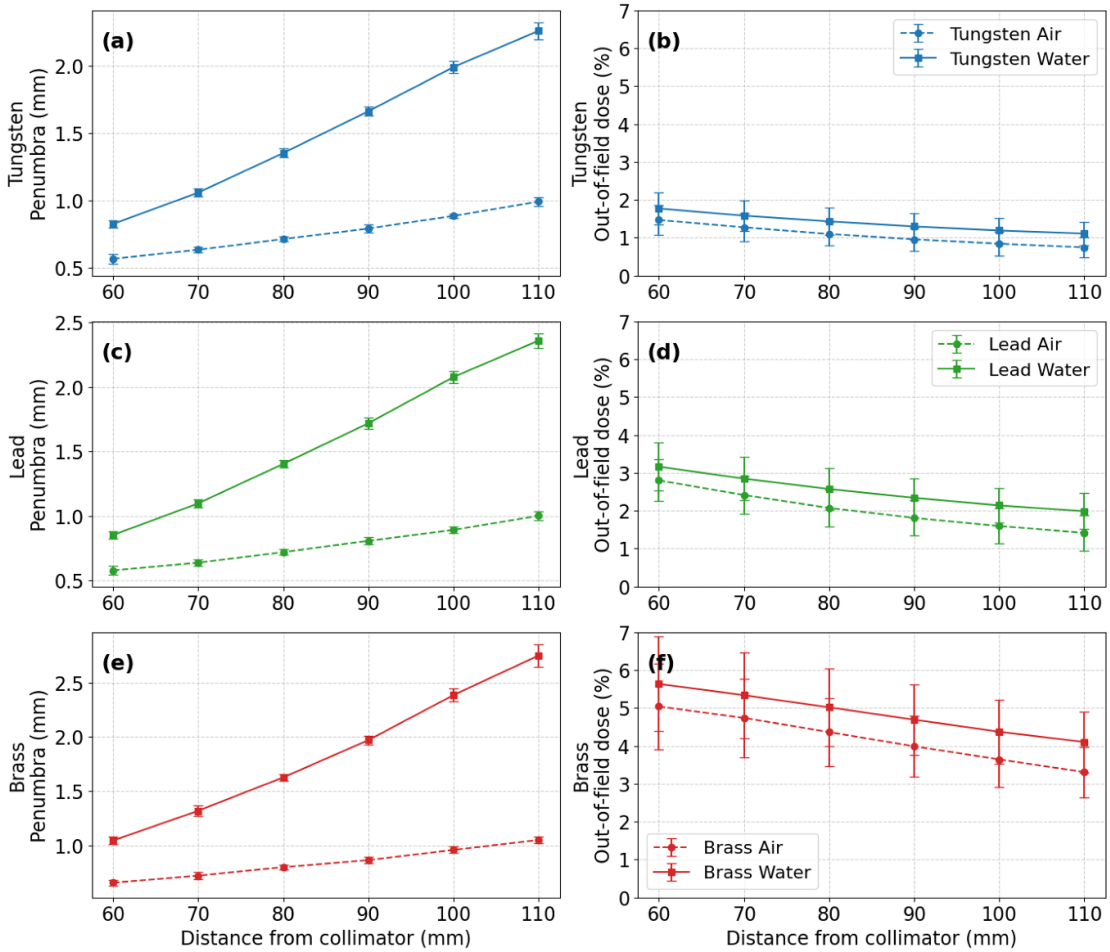

Figure 4. Beam penumbra and out-of-field dose for 20 mm tungsten, lead, and brass blocks under 200 MeV irradiation. Dashed lines represent simulations in air and solid lines represent simulations in water. The *x*-axis indicates the distance from the collimator, with the first film in water at a depth of 22 mm. Panels (a), (c), (e) on the left display the penumbra as a function of distance for tungsten, lead, and brass, respectively, while panels (b), (d), (f) on the right show out-of-field dose as a function of distance for the same materials.

$3.2 \pm 0.6\%$ to $2.0 \pm 0.4\%$ in water. Brass produced the widest beam penumbra and the highest out-of-field dose, with penumbrae in water ranging from 1.04 ± 0.03 mm to 2.7 ± 0.1 mm and out-of-field dose from $5.6 \pm 1.2\%$ to $4.1 \pm 0.8\%$.

The rate of penumbra increase in water was greater than in air. For the tungsten collimator in water the penumbra increased at a rate of 3.5% mm^{-1} from the collimator, while in air the penumbra increased at a rate of 1.5% mm^{-1}.

3.2. Experimental beam modeling

MC simulations for three setups were compared against film measurements. The results for the tungsten, lead, and brass collimators, simulated using a 200 MeV beam model with an initial Gaussian distribution of $\sigma = 40$ mm and varying angular divergence, are shown in figure 5. The optimal angular divergence for tungsten, lead, and brass was found to be 0.12°, 0.12°, and 0.14°, respectively, whereas the optimal beam size (σ) was found to be 4.07 mm, 4.10 mm, and 4.05 mm, respectively. Penumbrae values matched closely across all materials and distances with differences remaining within 0.03 mm for tungsten, 0.05 mm for lead and 2 mm for brass. At 60 mm from the collimator, the experimental penumbrae recorded on the films were 0.42 ± 0.08 mm for tungsten, 0.42 ± 0.07 mm for lead, and 0.41 ± 0.05 mm for brass, compared to corresponding MC values of 0.40 ± 0.06 mm, 0.41 ± 0.09 mm, and 0.45 ± 0.09 mm, respectively. Out-of-field dose predictions were consistently lower in the MC simulations compared to films. For tungsten, the average difference across all distances was 0.61%, with the largest difference of 0.88% at 60 mm. Lead showed an average difference of 0.95%, while brass demonstrated the poorest agreement, with out-of-field dose underestimated for a difference of 1.40% from the MC results. At 60 mm, film-measured out-of-field dose was $5.14 \pm 0.8\%$ for brass, compared to $4.44 \pm 0.9\%$ in the MC simulations.

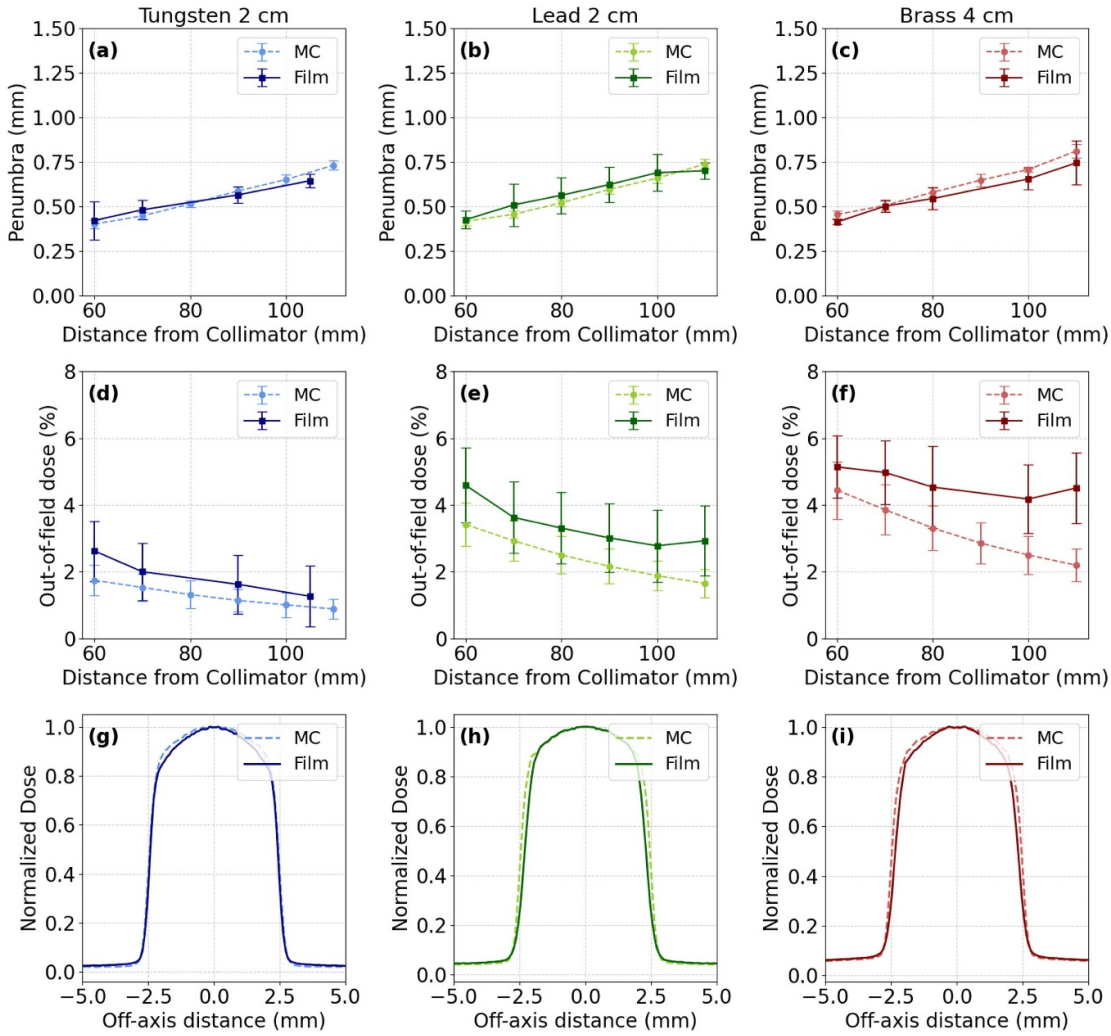

Figure 5. The first two rows show MC simulations and experimental film measurements of beam penumbrae for collimators made of (a) 20 mm of tungsten, (b) 20 mm of lead and (c) 40 mm of brass. Measured out-of-field dose on film for collimators made of (d) 20 mm of tungsten, (e) 20 mm of lead and (f) 40 mm of brass. The bottom row displays VHEE beam profiles at 70 mm from the (g) tungsten, (h) lead and (i) brass collimators for films and MC simulations.

Energy spectra scored along the CAX showed that collimation reduced the mean energy and broadened the spectral width for all materials (figure 6). The initial beam just upstream of the collimator had a mean energy of 199.4 MeV with a spread of 9.4 MeV. The energy distribution was extremely narrow, with the 5th percentile at 199.89 MeV with 90% of particles exceeding 199.92 MeV, indicating negligible spectral broadening. Downstream of the tungsten collimator, the beam had a mean energy of 165.4 MeV with an energy spread of 69.9 MeV. The 5th-percentile energy was $E_{\text{low}} = 3.65$ MeV, and the energy exceeded by 90% of particles was $E_{\text{high}} = 13.64$ MeV. For lead and brass, the mean energies were 148.6 MeV and 153.6 MeV with spreads of 79.4 MeV and 74.7 MeV, respectively. For lead, $E_{\text{low}} = 4.76$ MeV and $E_{\text{high}} = 13.31$ MeV and for brass, $E_{\text{low}} = 2.84$ MeV and $E_{\text{high}} = 8.53$ MeV.

Photon and neutron contributions to the out-of-field dose were quantified relative to both the peak CAX dose and the total out-of-field dose. For tungsten, photon contamination increased progressively with distance from the collimator, from $5.8 \pm 0.1\%$ of the out-of-field dose at 60 mm to $22.6 \pm 0.1\%$ at 110 mm (0.08%–0.17% of the peak dose). The neutron dose was $0.21 \pm 0.02\%$ of the out-of-field dose at 60 mm from the collimator (0.003% of the peak dose) and decreased with distance to $0.12 \pm 0.01\%$ of the out-of-field dose (0.001% of the peak dose) at 110 mm. For lead, photon contamination rose from $3.9 \pm 0.1\%$ to $17.7 \pm 0.1\%$ of the out-of-field dose between 60 mm and 110 mm (0.11%–0.26% of the peak dose). Neutrons from the lead collimator contributed $0.04 \pm 0.01\%$ of the out-of-field dose at 60 mm (0.001% of the peak dose). For brass, photon dose fractions similarly increased with depth, from $3.41 \pm 0.04\%$ to $12.58 \pm 0.07\%$ of the out-of-field dose (0.10%–0.23% of the peak). The neutron dose from the brass collimator was negligible, contributing less than 0.02% of the out-of-field dose.

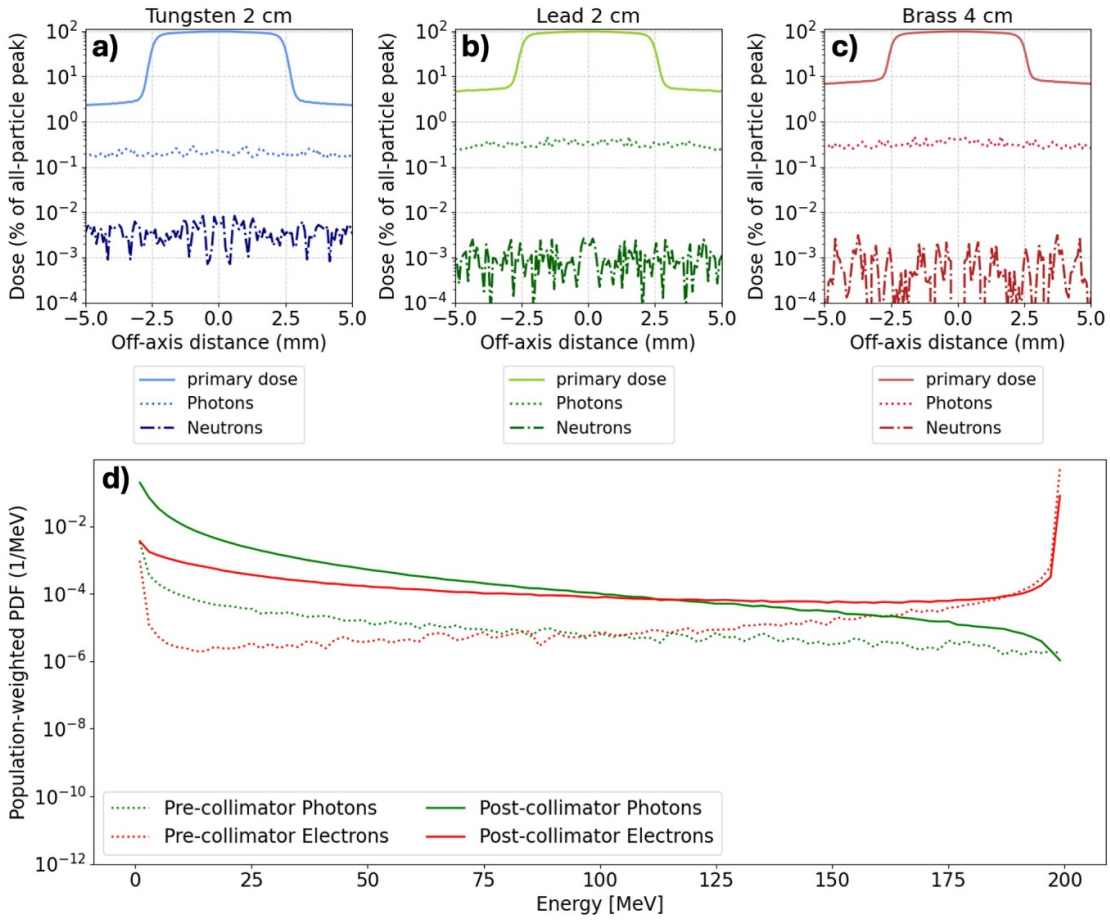

Figure 6. The top panels show the normalized lateral dose profiles scored at 10 mm downstream of the collimator for (a) 20 mm tungsten, (b) 20 mm lead, and (c) 40 mm brass. The graphs differentiate the primary dose (solid line) from contributions from photons (dotted line) and neutrons (dash-dotted line). The bottom panel (d) shows energy spectra produced by the 20 mm tungsten collimator for photons (green) and electrons (red) scored 5 mm upstream (dotted) and 5 mm downstream (solid) of the collimator.

3.3. Beam sensitivity tests

The influence of beam parameters (angular divergence, beam offset, and beam size) on collimated beam shaping was investigated using a 20 mm tungsten collimator at 200 MeV (figure 7).

Increasing beam divergence led to a steady broadening of the penumbra. The penumbra widened from 0.33 mm at 0.04° to 0.53 mm at 0.18°, representing a 0.20 mm increase at 60 mm. The effect was less pronounced at 110 mm distance where the penumbra rose from 0.63 mm to 0.91 mm at 110 mm, a 44% increase. In contrast, out-of-field dose remained effectively unchanged across divergence values in the tested parameter space. The out-of-field dose varied by less than 1% and remained within one standard deviation of the mean. These results indicate that increasing divergence primarily affects the beam-edge sharpness while leaving overall out-of-field dose unchanged.

Collimator misalignment along the axis perpendicular to the VHEE beam had the strongest influence on beam penumbra, particularly beyond a 2 mm lateral shift. At 60 mm from the collimator, the penumbra increased from 0.38 ± 0.02 mm for a centered beam to 1.03 ± 0.34 mm for a 3 mm offset. For each mm in increasing offset the penumbrae values rose by 30%–40% which was equivalent to an absolute 0.1–0.3 mm increase in penumbra. The out-of-field dose showed minimal variation with misalignment perpendicular to the beam.

Beam size had a modest but noticeable effect on the penumbra. At 60 mm from the collimator, the penumbra increased by 0.22 ± 0.05 mm as σ grew from 3.0 mm to 6.0 mm. The beam with a 3.0 mm σ was much smaller than the 5.0 mm collimator bore, resulting in a poorly collimated field that did not fully utilize the collimator aperture. Beam size had a greater impact on the out-of-field dose. At 60 mm from the collimator, the 3.0 mm beam size resulted in a out-of-field dose of $0.9 \pm 0.2\%$ compared to a beam size of 6.0 mm which showed a out-of-field dose of $2.3 \pm 0.6\%$.

Shifting the collimator along the beam axis demonstrated that moving the collimator farther from the film (−) increased the penumbra, while moving it closer (+) reduced it. At 60 mm distance, the

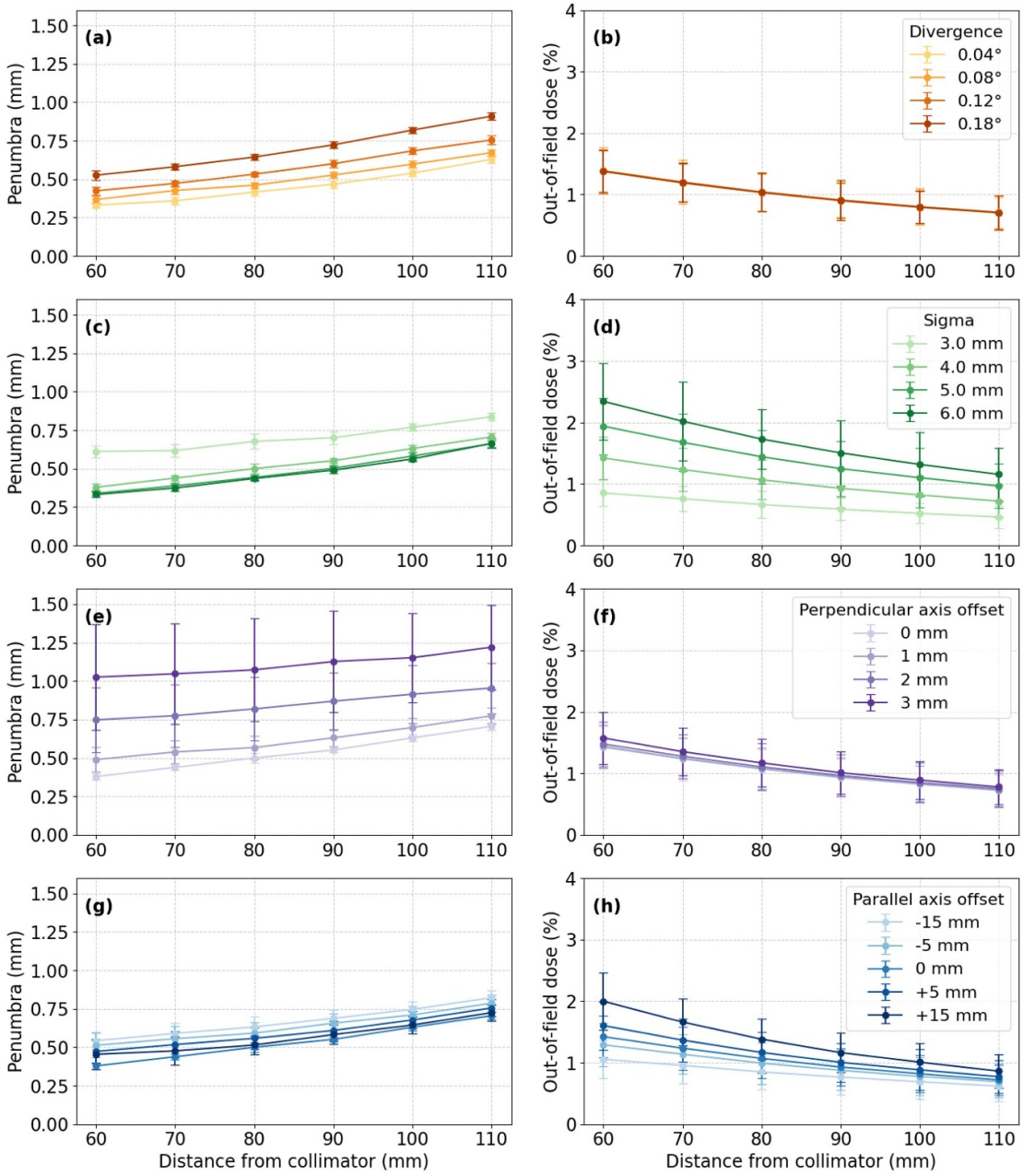

Figure 7. The effect of various beam parameters on beam penumbra and out-of-field dose for varying (a), (b) beam divergence, (c), (d) beam size, (e), (f) collimator misalignment perpendicular to the beam and (g), (h) parallel to the beam. Simulations were performed in air with a 20 mm tungsten collimator.

penumbra decreased from 0.54 ± 0.05 mm with a -15 mm shift to 0.45 ± 0.09 mm with a $+15$ mm shift. The out-of-field dose followed the opposite trend; as the collimator was positioned closer to the film, out-of-field dose increased. At -15 mm, the out-of-field dose at 60 mm distance was $1.05 \pm 0.31\%$, compared to $2.00 \pm 0.47\%$ when shifted to $+15$ mm. This indicates that reducing the gap between the collimator and scoring plane tightens the field edge but also increases the dose in the out-of-field region.

4. Discussion

To our knowledge, this study presents the first dedicated investigation of collimation for VHEEs, combining experimental measurements with MC simulations to characterize out-of-field dose, and penumbra behavior across different materials and geometries. The experimental results were used to inform and validate the simulation framework. These methods provide an assessment of how material composition

and thickness affect VHEE collimation, which is essential for guiding future collimator design in both preclinical and clinical systems. Based on the results of this study, the CLEAR facility has replaced its previous lead–steel collimator with a tungsten collimator.

4.1. Parameter study

The beam penumbra increased with distance from the collimator at a modest rate due to the minimal scatter in air. The out-of-field dose decreased with distance from the collimator. This behavior is attributed to the fact that the simulations and measurements were performed in air. Out-of-field dose in this context arises primarily from particles transmitted through the collimator and from those undergoing large-angle scattering. As the distance from the collimator increases, these particles diverge further from the central axis, thereby reducing their contribution to the measured out-of-field dose. In water, however, additional interactions such as multiple Coulomb scattering and energy loss would be expected to modify this behavior.

Increasing beam energy showed minimal changes in penumbra. The penumbra is primarily governed by multiple Coulomb scattering in the collimator material. Scattering angles are small for VHEEs and increasing the energy from 150 to 250 MeV therefore produces only a small change in lateral spread over the short distances considered here. As a result, the penumbra changes only slightly across this energy range.

Increasing the collimator thickness beyond 40 mm yielded only minor improvements in penumbra, regardless of collimator material. For the 20 mm thick collimator, brass exhibited a noticeably wider penumbra. Beyond this singular case, the penumbra remained relatively unchanged (< 0.11 mm) across the investigated parameter space. Differences in out-of-field dose were strongly material dependent. Tungsten achieved the lowest out-of-field dose, below 1.5%, due to its high atomic number and mass density, which effectively attenuated scattered electrons and suppressed transmission through the collimator body. Brass, having the lowest Z and mass density among the tested materials, produced the highest out-of-field dose. These findings suggest that in practical collimator design, collimator thickness should be optimized primarily for out-of-field dose control rather than incremental improvements in penumbra.

4.2. Experimental beam modeling

Several factors limited the accuracy of MC representation of the experimental conditions, and likely contributed to the observed mismatch in the out-of-field dose. When comparing absolute dose, MC values underestimated the out-of-field dose compared to the film-based results by approximately 13%–33% for the first film at 60 mm depth, with the discrepancy gradually decreasing at larger depths.

A portion of this error likely stems from uncertainties in the measured delivered beam. As described in section 2.4.4, variations in beam size or collimator positioning can increase the out-of-field dose. Additionally, the mismatch in the out-of-field dose may be partly due to particle-type dependence of the radiochromic film response. The film was calibrated using 5.5 MeV electrons, which produce a lower optical density response than photons (Sorriaux *et al* 2013). As a result, bremsstrahlung photons generated in the collimator may lead to an overestimation of dose in the film measurement, particularly in the out-of-field region. For the geometries investigated, bremsstrahlung contributed up to 7.5% of the out-of-field dose at the film nearest to the collimator.

The simulations also predicted a negligible neutron component originating from photonuclear reactions caused by bremsstrahlung photons with energies exceeding $\sim$ 10 MeV. The neutron dose was less than 0.001% of the peak dose on the CAX for brass and 0.003% for tungsten. While radiochromic films are not typically used to record neutron dose, studies have shown that for neutrons above 1 MeV, the dose may be underestimated as being less than half of the true dose. Additionally, neutrons may contribute to secondary activation and should be considered in future shielding and radiation-safety designs for clinical VHEE systems.

Although spectrometry measurements of collimator induced radioactivity were performed in this study, these results were excluded from the main analysis due to uncertainties in both the delivered dose to each collimator and the precise collimator composition. Based on recorded activation products, the tungsten collimator material was identified as thoriated tungsten. Commercial radiotherapy collimators use non-thoriated high-purity tungsten, resulting in lower activation levels in clinical systems. Notably, Th-232 with a specific activity of 168.3 ± 53.2 Bq was detected. The isotopes with the next highest specific activities generated from the tungsten collimator were identified as W-187 and Ni-57 which had specific activities of 10.5 ± 0.4 Bq and 6.1 ± 0.3 Bq, respectively. Activated lead produced Pb-203 with a specific activity of 1.3 ± 0.1 Bq, while brass was found to predominantly yield Cu-67 (5.6 ± 0.5 Bq) and Zn-65 (1.1 ± 0.1 Bq), the latter being notable for its long half-life of 244 d.

4.3. Beam sensitivity tests

The experimental nature of the CLEAR facility introduces fluctuations in beam charge, position, and divergence between experimental runs. These instabilities contributed to small variations in measured out-of-field dose and penumbra across irradiations. While daily open beam normalization helped reduce differences between irradiation days, drifts occurring during the same day remained unavoidable. On the other hand, the CLEAR beamline is highly flexible, supporting a wide range of user experiments, and offering extensive control over beam parameters. Configurability of an experimental beamline comes at the cost of stability, where each adjustable component is more susceptible to drift. In contrast, a clinical VHEE beamline would operate within a fixed, tightly controlled parameter set, minimizing such sources of instability.

The MC simulations revealed that the penumbra and out-of-field dose of collimated VHEE beams were highly sensitive to the intrinsic beam properties. Increasing beam divergence produced a broadening of the penumbra while having no effect on the out-of-field dose. For the conducted tests, the size of the beam incident on the collimator was kept constant. The increase in divergence altered the angle at which particles grazed the collimator edges, thereby impacting the penumbra. The out-of-field dose remained unaffected as the proportion of the beam striking the collimator, and consequently the amount transmitted or scattered through it, remained effectively constant. This is further supported by the beam size tests, which showed that as the beam size increased, the out-of-field dose also increased. The penumbra exhibited little change with increasing beam size, except for small beam sizes. For a beam of $\sigma = 3.0$ mm, the out-of-field dose was noticeably higher. This may be attributed to the beam size being smaller than the collimator aperture by 2 mm, resulting in insufficient collimation.

The results indicate that precise control of beam optics will be essential for consistent and reproducible VHEE field shaping in future clinical systems. Additionally, the simulations showed that small lateral collimator misalignment of only 2–3 mm significantly increased the penumbra width. Although the effect may be reduced for larger beams that were outside the scope of this study, active beam-steering feedback may still be important to maintain a consistently sharp penumbra.

4.4. Recommendations for VHEE collimation

For VHEE beams delivered at UHDRs, both collimator heating and activation become important design and safety considerations for collimator systems. Each pulse deposits substantial energy within the collimator material, which can lead to localized heating. The magnitude of heating depends strongly on the beam energy, pulse repetition rate, and collimator thickness (Meier and Duerre 1976, Wang *et al* 2017). Tungsten has a high thermal conductivity and is therefore relatively resistant to damage; however it may still experience temperature rise under sustained irradiation (Callister and Rethwisch 2019). Lead is a poor thermal conductor, which results in localized heating. Furthermore, lead has a much lower melting point and mechanical strength, making it prone to deformation. Brass exhibits a slightly better thermal conductivity, resulting in more uniform heating across its volume than lead (Callister and Rethwisch 2019). These mechanical properties are key considerations in collimator design and indicate that brass or tungsten would best serve as collimators for a VHEE system.

Activation is an important consideration for VHEE systems, particularly in contexts where secondary photon energies exceed approximately 10 MeV. At these energy levels, bremsstrahlung photons can induce photonuclear reactions, such as (γ,n) and $(\gamma,2n)$, in materials with high atomic numbers, leading to the generation of residual isotopes. Among various materials, tungsten is especially prone to activation because of its high atomic number and significant photonuclear cross section (Kawano 2020). In contrast, brass, which is primarily made up of copper and zinc, exhibits greater resistance to such processes (Kawano 2020). While the levels of activation may be low relative to the peak dose, they become important for systems operated continuously or at high pulse repetition rates. Cumulative exposure from ongoing operations can lead to a noticeable increase in residual activity. Characterizing activation through systematic post-irradiation spectroscopy and investigation of activation products through MC simulations will be a key step to establishing a safe clinical VHEE system.

Based on the results of this study, which demonstrate that tungsten provides sharp penumbra while minimizing out-of-field dose, the authors propose that future VHEE collimation should utilize tungsten collimators. Although lead provides comparable penumbra and less than 1% out-of-field dose at 60 mm thickness for 200 MeV, its poor mechanical strength and susceptibility to deformation make it a less suitable collimator material. For tungsten, the main consideration is the potential for activation and neutron production, however, the simulations in this study demonstrated only low levels of neutron generation. A plausible clinical VHEE collimation approach could employ tungsten multileaf collimator analogous

to those used in conventional linacs. In contrast, machining custom apertures from solid tungsten is both technically challenging and prohibitively expensive to manufacture. In this study, a 60 mm tungsten collimator achieved out-of-field dose below 0.2%. As modern linacs already employ tungsten leaves of approximately 50–75 mm thickness, this would be within a reasonable range for construction (Hariri 2010).

5. Conclusion

This study presents experimental and MC characterization of beam collimation for very high- energy electrons. Collimator performance was found to depend strongly on material, thickness, and beam properties. Tungsten provided the sharpest field edges and lowest transmission, while brass produced broader penumbra and higher out-of-field dose. In this study, beam stability and alignment were identified as additional factors affecting post-collimation beam sharpness; small changes in beam divergence or positioning may increase VHEE beam penumbra widths by up to 0.65 mm and the out-of-field dose by up to 1.49%.

Acknowledgment

The authors would like to acknowledge funding from the NSERC Canada Graduate Research Scholarship program, NSERC Discovery Grants and the Canada Research Chairs program. This research was enabled by support provided by Calcul Québec (calculquebec.ca) and the Digital Research Alliance of Canada (alliancecan.ca). Additionally, the authors would like to acknowledge Chris Secord for machining the collimators used in the experimental studies.

Data availability statement

The data cannot be made publicly available upon publication because they are not available in a format that is sufficiently accessible or reusable by other researchers. The data that support the findings of this study are available upon reasonable request from the authors.

Author contributions

Jade Fischer 0009-0000-8862-1263
Conceptualization (lead), Data curation (equal), Formal analysis (lead), Investigation (lead), Methodology (lead), Validation (lead), Visualization (lead), Writing – original draft (lead), Writing – review & editing (lead)

Antonio Gilardi
Data curation (equal), Resources (supporting)

Alexander Malyzhenkov
Data curation (equal)

Pierre Korysko 0000-0002-7878-2298
Data curation (equal)

Alexander Hart 0000-0002-0547-5887
Conceptualization (supporting), Data curation (supporting)

Vilde Rieker
Data curation (supporting), Writing – review & editing (supporting)

Joseph Bateman 0000-0002-5967-6748
Data curation (supporting)

Wilfrid Farabolini
Data curation (supporting)

Roberto Corsini
Data curation (supporting), Project administration (equal), Supervision (supporting)

Manjit Dosanjh 0000-0003-1378-349X
Data curation (supporting), Project administration (equal), Supervision (supporting)

Magdalena Bazalova-Carter 0000-0002-9365-2889
Funding acquisition (lead), Project administration (lead), Supervision (lead), Writing – review & editing (supporting)

References

Bazalova-Carter M *et al* 2015 Comparison of film measurements and Monte Carlo simulations of dose delivered with very high-energy electron beams in a polystyrene phantom *Med. Phys.* **42** 1606–13
Bazalova-Carter M, Qu B, Palma B, Hårdemark B, Hynning E, Jensen C, Maxim P G and Loo B W 2015 Treatment planning for radiotherapy with very high-energy electron beams and comparison of VHEE and VMAT plans *Med. Phys.* **42** 2615–25
Boyer A, Biggs P, Galvin J, Klein E, LoSasso T, Low D, Mah K and Cedric C 2001 Basic applications of multileaf collimators *Technical Report* American Association of Physicists in Medicine
Callister W D and Rethwisch D G 2019 *Fundamentals of Materials Science and Engineering : An Integrated Approach* (Wiley)
Chen H, Matysiak W, Flampouri S, Slopsema R and Li Z 2014 Dosimetric evaluation of hybrid brass/stainless-steel apertures for proton therapy *Phys. Med. Biol.* **59** 5043–60
Clements N and Bazalova-Carter M 2024 Monte Carlo calculated absorbed-dose energy dependence of EBT3 and EBT4 films for 5–200 mev electrons and 100 KeV–15 MeV photons *J. Appl. Clin. Med. Phys.* **25** e14529
Clements N, Esplen N M, Bateman J J, Robertson C, Dosanjh M, Korysko P, Farabolini W, Corsini R and Bazalova-Carter M 2024 Mini-grid radiotherapy on the clear very-high-energy electron beamline: collimator optimization, film dosimetry and Monte Carlo simulations *Phys. Med. Biol.* **69** 055003
Clements N, Esplen N and Bazalova-Carter M 2023 A feasibility study of ultra-high dose rate mini-grid therapy using very-high-energy electron beams for a simulated pediatric brain case *Phys. Med.* **112** 102637
DesRosiers C, Moskvin V, Bielajew A F and Papiez L 2000 150-250 MeV electron beams in radiation therapy *Phys. Med. Biol.* **45** 1781–805
Faddegon B, Ramos-Méndez J, Schuemann J, McNamara A, Shin J, Perl J and Paganetti H 2020 The TOPAS tool for particle simulation, a Monte Carlo simulation tool for physics, biology and clinical research *Phys. Med.* **72** 114–21
Farr J, Grilj V, Malka V, Sudharsan S and Schippers M 2022 Ultra-High Dose Rate Radiation Production and Delivery Systems Intended for Flash *Medical Physics* vol 49 (Wiley) pp 4875–911
Fischer J, Whitmore L, Desrosiers C, Sheehy S and Bazalova-Carter M 2024 Very high-energy electrons as radiotherapy opportunity *Eur. Phys. J. Plus* **139** 728
Giguére C, Hart A, Bateman J, Korysko P, Farabolini W, LeChasseur Y, Bazalova-Carter M and Beaulieu L 2025 Radiation damage and recovery of plastic scintillators under ultra-high dose rate 200 MeV electrons at CERN CLEAR facility *Phys. Med. Biol.* **70** 075018
Glinec Y, Faure J, Malka V, Fuchs T, Szymanowski H and Oelfke U 2006 Radiotherapy with laser-plasma accelerators: Monte Carlo simulation of dose deposited by an experimental quasimonoenergetic electron beam *Med. Phys.* **33** 155–62
Hariri S and Shahriari M 2010 Suggesting a new design for multileaf collimator leaves based on Monte Carlo simulation of two commercial systems *J. Appl. Clin. Med. Phys.* **11** 173–85
Hart A *et al* 2024 Plastic scintillator dosimetry of ultrahigh dose-rate 200 MeV electrons at clear *IEEE Sens. J.* **24** 14229–37
Hyer D E, Bennett L C, Geoghegan T J, Bues M and Smith B R 2021 Innovations and the use of collimators in the delivery of pencil beam scanning proton therapy *Int. J. Part. Ther.* **8** 73–83
Jaccard M, Petersson K, Buchillier T, Germond J F, Durán M T, Vozenin M C, Bourhis J, Bochud F O and Bailat C 2017 High dose-per-pulse electron beam dosimetry: usability and dose-rate independence of EBT3 Gafchromic films: usability *Med. Phys.* **44** 725–35
Jursinic P A and Mueller R 1997 A sector-integration method for calculating the output factors of irregularly shaped electron fields *Med. Phys.* **24** 1765–9
Kawano T *et al* 2020 IAEA photonuclear data library 2019 *Nucl. Data Sheets* **163** 109–62
Korysko P, Dosanjh M, Bateman J, Robertson C, Corsini R, Farabolini W, Aksoy A, Malyzhenkov A, Rieker V Sjobak K and 2023 The clear user facility:a review of the experimental methods and future plans
Law J W, Santos A and Penfold S 2025 Radiological assessment of Cerrobend and tungsten carbide as aperture materials in proton therapy *Phys. Med.* **137** 105084
Lee U S, Kim S W, Shin J B, Jeong C, Goh Y, Park M J, Kwak J, Song S Y and Cho B 2025 Intraoperative radiotherapy iort applicators for treatment of small skin lesions a phantom and planning study *Sci. Rep.* **15** 5499
Li H, Zha H, Lin X, Gao Q, Liu F, Shi J and Chen H 2024 Design of a 100-MeV compact VHEE beam line in tsinghua university *Front. Phys.* **12** 1496272
Maharaj K D, Dass J, Ibrahim M, Mahmood T and Rowshanfarzad P 2024 Peripheral doses beyond electron applicators in conventional c-arm linear accelerators: a systematic literature review *Technol. Cancer Res. Treat.* **23** 15330338241239144
Meier R W and Duerre K H 1976 Thermal stress analysis of tungsten collimators heated by high-energy proton beams *Technical Report* University of California
Palma B, Bazalova-Carter M, Hårdemark B, Hynning E, Qu B, Loo B W and Maxim P G 2016 Assessment of the quality of very high-energy electron radiotherapy planning *Radiother. Oncol.* **119** 154–8
Papiez L, DesRosiers C and Moskvin V 2002 Very high energy electrons (50–250 MeV) and radiation therapy *Technol. Cancer Res. Treat.* **1** 105–10
Perl J, Shin J, Schümann J, Faddegon B and Paganetti H 2012 TOPAS: an innovative proton Monte Carlo platform for research and clinical applications *Med. Phys.* **39** 6818–37

Robertson C, Corsini R, Farabolini W, Gerbershagen A, Korysko P, Latina A, Malyzhenkov A and Dosanjh M 2026 Demonstration and characterisation of a novel dual-scattering system for very high energy electrons *Nucl. Instrum. Methods Phys. Res. A* **1082** 170943

Ronga M G, Cavallone M, Patriarca A, Leite A M, Loap P, Favaudon V, Créhange G and Marzi L D 2021 Back to the future: very high-energy electrons (VHEES) and their potential application in radiation therapy *Cancers* **13** 4942

Ronga M G, Gesualdi F, Bonfrate A, Patriarca A, Ferrand R, Créhange G, Buvat I and Marzi L D 2025 Comparison of secondary radiation dose between pencil beam scanning and scattered delivery for proton and VHEE radiotherapy *Med. Phys.* **52** 4775–84

Schuler E, Eriksson K, Hynning E, Hancock S L, Hiniker S M, Bazalova-Carter M, Wong T, Le Q T, Loo B W and Maxim P G 2017 Very high-energy electron (VHEE) beams in radiation therapy; treatment plan comparison between VHEE, VMAT and PPBS *Med. Phys.* **44** 2544–55

Sorriaux J, Kacperek A, Rossomme S, Lee J A, Bertrand D, Vynckier S and Sterpin E 2013 Evaluation of Gafchromic® EBT3 films characteristics in therapy photon, electron and proton beams *Phys. Med.* **29** 599–606

Subiel A *et al* 2014 Dosimetry of very high energy electrons (VHEE) for radiotherapy applications: using radiochromic film measurements and Monte Carlo simulations *Phys. Med. Biol.* **59** 5811–29

Wang J, Trovati S, Borchard P M, Loo B W, Maxim P G and Fahrig R 2017 Thermal limits on mv x-ray production by bremsstrahlung targets in the context of novel linear accelerators *Med. Phys.* **44** 6610–20

Whitmore L, Mackay R I, Herk M V, Jones J K and Jones R M 2021 Focused vhee (very high energy electron) beams and dose delivery for radiotherapy applications *Sci. Rep.* **11** 14013

Whitmore L, Mackay R I, van Herk M, Korysko P, Farabolini W, Malyzhenkov A, Corsini R and Jones R M 2024 Cern-based experiments and Monte-Carlo studies on focused dose delivery with very high energy electron (VHEE) beams for radiotherapy applications *Sci. Rep.* **14** 11120

Yeboah C, Sandison G A and Moskvin V 2002 Optimization of intensity-modulated very high energy (50-250 MeV) electron therapy *Phys. Med. Biol* ***47*** 1285–1301

Zhang G, Wang J, Wang Y and Peng H 2021 Proton flash: passive scattering or pencil beam scanning? *Phys. Med. Biol.* **66** 03NT01

Zhou G 2020 Mechanisms underlying flash radiotherapy, a novel way to enlarge the differential responses to ionizing radiation between normal and tumor tissues *Radiat. Med. Prot.* **1** 35–40